Nitrobenzoic acid-functionalized gold nanoparticles: DET promoter of multicopper oxidases and electrocatalyst for NAD-dependent glucose dehydrogenase

Noémie Lalaoui, Kilian Gentil, Ilyass Ghandari, Serge Cosnier, Fabien Giroud

Nitrobenzoic acid-functionalized Gold Nanoparticles: DET promoter of Multicopper Oxidases and Electrocatalyst for NAD-Dependent Glucose Dehydrogenase

Noémie Lalaoui[a,*], Kilian Gentil[a], Ilyass Ghandari[a], Serge Cosnier[b], Fabien Giroud[b,*]

[a] Université de Bretagne Occidentale, CNRS, CEMCA UMR 6521, F-29238 Brest, France

[b] Univ. Grenoble Alpes, CNRS, DCM UMR 5250, F-38000 Grenoble, France

Abstract

We report the synthesis of coated gold nanoparticles with nitrobenzoic moieties (AuNPs-TNB). They displayed small and narrow size distribution (2 nm) as shown by TEM imaging. These functionalized AuNPs-TNB were physically adsorbed on multi-walled carbon nanotubes (MWCNTs) electrodes. Their stable adsorption was monitored by electrochemical methods. The stability of the activated hydroxylamine layer was enhanced compared to the adsorption of the dinitro precursor onto the CNTs layer. Unactivated AuNPs-TNB enhanced the oxygen reduction reaction catalyzed by multicopper oxidases through increased aromatic and electrostatic interactions with limiting current densities higher than 500 µA cm^{-2}. Next, the electrocatalytic properties of the active form toward the oxidation of the reduced form of nicotinamide adenine dinucleotide (NADH) with low overpotential was shown at near neutral pH. Associated with a NAD-dependent glucose dehydrogenase, the bioelectrodes were assessed for glucose electrooxidation. A complete glucose/O_2 enzymatic fuel cell was developed based on unactived and activated AuNPs as cathodic DET promoter and anodic electrocatalyst respectively. The nanostructured assembly exhibited efficient glucose oxidation with current densities of 450 µA cm^{-2} in high glucose concentration and O_2 saturated conditions. In concentration close to those found in physiological fluids (0.04 to 4.00 mmol L^{-1}), the enzymatic biofuel cell displayed a linear range for glucose concentration and a low limit of detection (2.5 ± 0.9 µmol L^{-1}).

1. Introduction

Bioelectrocatalysis is used in bioanalysis, bioenergy and green synthesis. It involves the use of redox proteins to undergo the oxidation or reduction of specific targeted substrates for their quantification, clean electricity generation or their conversion to higher value-added chemicals [1]. For example, glucose is a widely studied substrate in this field because it is an affordable, non-toxic and stable analyte. In physiological conditions, glucose level can be associated to several health disorders such as diabetes, a higher risk to develop cancer [2] and could be linked to worse prognosis for patients with COVID-19 [3]. Usually, its monitoring is performed from blood samples. It can also be found in other physiological fluids such as saliva [4], tears [5], sweat [6], urine [7], or breath condensate [8]. It has been shown that to some

extent, glucose level in these fluids can be fluctuating in the same manner as blood glucose, and consequently its quantification in external body fluids can be correlated with health conditions. Hence, it is still of interest to propose new strategies to help in monitoring glucose level in physiological ranges (i.e. 50 µmol L^{-1} to 4.0 mmol L^{-1}) for fast and non-invasive biosensing. Glucose can be oxidized enzymatically by several oxidoreductases. Among them, the NAD-dependent glucose dehydrogenase (GDH) utilizes nicotinamide adenine dinucleotide (NAD^+) as cofactor. This NAD^+ prosthetic group is shared by more than 300 other dehydrogenases involved in several metabolic pathways such as glycolysis and Krebs cycle. Hence, it makes GDH an interesting model for point of care diagnostic but also for every other NAD-dependent enzymes (used in energy conversion or green synthesis).

Unlike other cofactors, NADH/NAD^+ is loosely bound to the proteins and usually has to be added into the medium. Some literature reports its direct incorporation in the modified matrices to increase its local concentration [9,10]. It has a low redox potential ($E°'$ = -0.560 V vs. SCE at pH 7.0) but high overpotentials are required for its electrochemical conversion at electrode surfaces. As a result, the use of electrocatalysts like Meldola blue [11], Azure dyes [12,13] or quinones [14] is recommended to favor the reaction. Nitroaromatics are also known as good catalysts for NAD^+ regeneration. Literature reports on the number of activated nitro groups, the number of substitution and the mechanism of activation of the catalytically active form [15,16]. Due to their chemical structures, nitroaromatics have been immobilized on different electrode materials and with different methodologies such as adsorption on 2D surfaces [16], 3D matrices [17], functionalization of polymers [18], non-covalent adsorption (with high π-π stacking affinity with CNTs) [19,20] and covalent bonding through amide [21] or Au-S bond formation [15].

Additionally, we have previously shown that the increased aromaticity and electrodonating groups due to the specific structure of carboxylated nitroaromatics can improve the orientation of multicopper oxidases (MCOs) such as laccase (Lc) and bilirubin oxidase (BOx) onto CNTs films with no NADH cross-reaction possible when the nitro group is not activated in a first step [19].

This report focuses on the synthesis of gold nanoparticles (AuNPs) decorated with nitro groups and their direct contribution to enhance electrocatalysis of ORR and NADH oxidation. Gold substrates have been used previously in various studies as electronic bridges for enzyme "wiring" [22] and for the immobilization of electrocatalysts containing disulfide bonds [23]. Herein, we present their utilization along with the laccase, bilirubin oxidase for ORR and the NAD-dependent model GDH for glucose electrooxidation as a proof of concept. AuNPs characterization was carried with spectroscopy and microscopy techniques to determine their size and to validate the synthesis of the nanoparticles with a thiol capping ligand bearing a nitro group. Unactivated AuNPs-TNB were first assessed for MCO orientation to improve ORR on CNTs films. Next, the nitro group was activated electrochemically to form the active

hydroxylamine/nitroso couple responsible for NADH oxidation. Associated with a CNT matrix and the GDH, the nanocomposite displayed good electrocatalytic properties for glucose oxidation reaching 400 µA cm^{-2} when the substrate was saturating the enzyme (>50 mmol L^{-1} glucose) at low potential. Finally, the complete assembly forming an enzymatic fuel cell, it was proposed as a device for glucose detection and quantification. It displayed linear relationships in the physiological glucose concentration regions that could potentially be useful for glucose sensing from external body fluids with minimum handling (i.e. no dilution).

2. Experimental details

2.1. Materials

5,5'-dithio-bis(2-nitrobenzoic acid) (DTNB), gold tetrachloride ($HAuCl_4$), sodium borohydride ($NaBH_4$), citric acid, sodium phosphate dibasic, nicotinamide adenine nucleotide (reduced form, NADH), nicotinamide adenine dinucleotide (hydrate, NAD^+), NAD-dependent glucose dehydrogenase (from *Pseudomonas* sp., E.C. 1.1.1.47, activity ≥ 200 U mg^{-1}), laccase (from *Trametes versicolor*, E.C. 1.10.3.2, activity ≥ 10 U mg^{-1}), BOx (from *Myrothecium verrucaria*, E.C. 1.3.3.5, activity ≥ 15 U mg^{-1}), glucose, ethanol, methanol (MeOH) and 1-methyl-2-pyrrolidone (NMP) were obtained from Merck (Sigma Aldrich) and used as received. Ascorbic acid, dopamine hydrochloride were purchased from Fisher Scientific. Uric acid was purchased from Alfa Aesar. Commercial grade thin Multi-Walled Carbon Nanotubes (9.5 nm diameter, 1.5 µm long, purity > 90 %) were obtained from Nanocyl and used as received.

2.2. Synthesis of TNB coated AuNPs (AuNPs-TNB)

Under argon, 0.15 mL of $HAuCl_4$ solution (215 µmol) was mixed with 60 mL of MeOH and 111 mg (280 µmol) of DTNB. Then, a freshly prepared solution of $NaBH_4$ (137 mg, 3.64 mmol) in 45 mL of MeOH was added slowly during half an hour and under vigorous stirring. Upon addition, the initial yellow solution became brown. The solution was stirred under argon for 24 h at room temperature. After this time, the solution was concentrated in vacuum until precipitation of the particles, which were collected by centrifugation (Jouan B4i). The solid product was washed by sonication /centrifugation in ethanol until no traces of free ligands were found from thin layer chromatography experiments and then dried under vacuum at 40°C.

2.3. Characterization methods

UV-Vis, FT-IR. UV-vis spectra were obtained from methanol solution with an optic fiber probe purchased from Ocean Optics. Infrared (IR) spectra were recorded on a platinum ATR Vertex 70 BRUKER spectrometer.

TEM. For morphology and size analysis of AuNPs, one aliquot of 0.5 mg mL^{-1} AuNPs-TNB in MeOH was prepared. Droplets (4 µL) were deposited onto glow-discharged carbon-coated 200 mesh copper grids and allowed to air-dry. The preparations were observed using a JEOL JEM 2100-Plus transmission electron microscope (TEM) operating at 200 kV. Images were recorded with a Gatan Rio 16 digital camera.

X- ray Photoelectron Spectroscopy. XPS data was obtained using an ESCALAB 250 from Thermo Scientific with a monochromated Al Kα band (1486.6 eV) as the excitation source. The diameter of the surface spot analyzed was 500 µm. Survey spectra were recorded from 0 to 1200 eV and referenced to the sp2 carbon energy contribution (C=C) C1s at 284.4 eV. The charge was compensated by an electron beam (-2 eV).

Electrochemistry. Glassy carbon electrodes (Ø = 3 mm) were obtained from ALS Co. (Japan) and HTDS (France). Prior to modification, the electrodes were polished with a 2 µm diamond paste purchased from Presi (France) and rinsed successively with water and ethanol and left to sonicate for 5 min in ethanol. The electrochemical characterizations for each electrode were carried out in a three-electrode electrochemical cell using Biologic SP200, VMP3 Multi Potentiostats with EC-lab software or an Autolab potentiostat with Nova software. A platinum wire and a saturated calomel electrode (SCE) electrode served as the counter electrode and reference electrode respectively. All potentials are referred to the SCE reference electrode. McIlvaine (McIl) buffer solutions with pH range [$3.0 \leq pH \leq 8.0$] were prepared from 0.1 mol L^{-1} citric acid and 0.2 mol L^{-1} Na_2HPO_4 stock solutions and used as supporting electrolytes for electrochemical characterizations of the AuNPs-TNB and GDH/AuNPs-TNB electrodes. During the irreversible reduction of NO_2 groups, the electrolyte was purged with argon (Ar) for 10 min. Distilled water was passed through a Milli-Q water purification system (Millipore, 18MΩ).

2.4. Electrodes Preparations

AuNPs-TNB/MWCNT modified electrodes. MWCNT films were prepared from a 3.0 mg mL^{-1} suspension in NMP kept for 30 min under sonication and finally shacked vigorously before pipetting. 20 µL of the black suspension was deposited onto glassy carbon electrode (GCE) and the solvent was removed under vacuum leading to the formation of a MWCNTs layer with a geometric surface area of 0.125 cm^2. The MWCNTs electrodes were incubated in 100 µL AuNPs-TNB solution (0.5 mg mL^{-1} in MeOH) for 12 h, thoroughly rinsed with MeOH and deionized water to remove any loosely adsorbed nanoparticles and then dried in air. Before electrochemical testing, the electrodes were soaked into McIlvaine buffer to equilibrate. (*step 1*)

Multicopper-based bioelectrodes. After *step 1*, AuNPs-TNB/MWCNTs modified electrodes were incubated in 50 µL of laccase or bilirubin oxidase solution (2.5 mg mL^{-1} in McIl pH 5.0 or 7.0, respectively) overnight at 4 °C. Before testing, electrodes were thoroughly rinsed with deionized water and soaked in fresh McIlvaine buffer solution to equilibrate.

NAD-dependent glucose dehydrogenase-based bioelectrodes. After the previous step, AuNPs-TNB/MWCNTs modified electrodes were incubated in 50 µL of GDH solution (1 mg mL^{-1} in McIl pH 7.0) overnight at 4°C. Before testing, electrodes were thoroughly rinsed with deionized water and soaked in fresh McIlvaine buffer solution (pH 7.0) to equilibrate. BSA-modified electrodes were adapted from this method by substitution of GDH with the non-redox active BSA.

3. Results and discussion

3.1. Synthesis and physical characterization of AuNPs-TNB

Functionalized gold nanoparticles were obtained from a mixed solution of $AuCl_4^-$, the capping agent DTNB in MeOH and the addition of the reducing agent $NaBH_4$ (**Scheme 1**). The formation of the particles was assessed immediately from the change of the bright yellow solution to a dark brown solution.

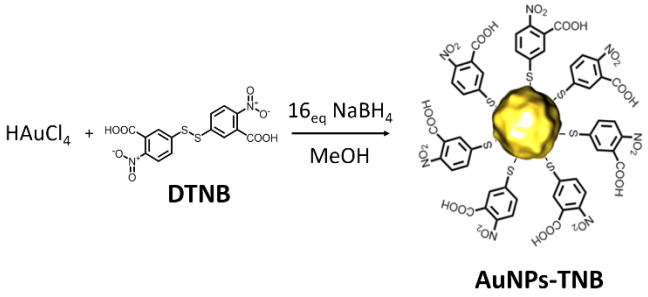

Scheme 1: Schematic representation of the AuNPs-TNB nanoparticles synthesis in MeOH

UV-Visible and FT-IR spectroscopies both confirmed the synthesis of the nanoparticles. The UV-Vis spectra of the AuNPs-TNB displayed a new band at λ = 395 nm while the characteristic band associated to DTNB completely disappeared (λ = 306 nm) (**Figure S1A**). The UV-Vis spectra did not show an usual plasmon band (near 520 nm), indicating that most particles were below ca. 3 nm in size [24].

FT-IR spectra (**Figure S1B**) for AuNPs-TNB showed similar peaks found in the DTNB precursor (υ = 500 to 1100 cm^{-1} for aromatic =C-H; υ = 1210 cm^{-1} for -C-O stretching; υ = 1320, 1560 cm^{-1} for N-O stretching; υ = 1610 cm^{-1} for C=O stretching; υ = 2985 cm^{-1} for =C-H stretching). The large band in the DTNB spectra (υ = 2200 to 3400 cm^{-1}) disappeared while a new large band was found at higher wavenumber (υ = 2750 to 3700 cm^{-1}) for the nanoparticles samples. This shift was still attributed to various O-H stretching mode and had been documented for other carboxylate capping ligand and hydrogen bonding with solvent

molecules [25]. Also, the merging and decrease in peak intensity could be attributed to the ordering of TNB molecule at the AuNP surface similarly to π-π stacking interactions [26]. Next, TEM imaging was performed in order to determine size and size distribution of the AuNPs-TNB population. The data confirmed the small and narrow size of the AuNPs assumed from UV-Vis spectra. The diameter of the AuNPs were in the range of 1.6 ± 0.3 nm and were relatively monodisperse as shown by the distribution curve (**Figure 1**).

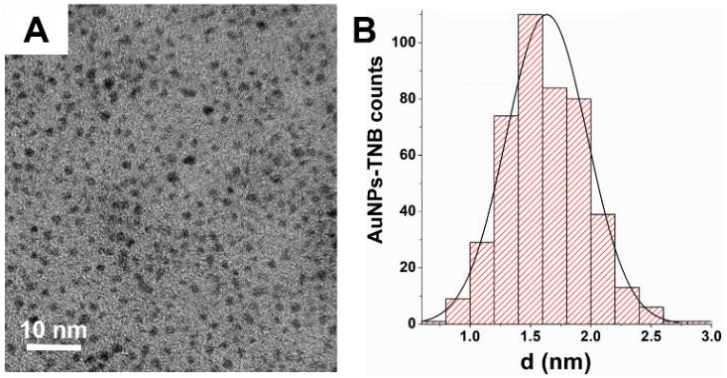

Figure 1: (A) TEM image of AuNPs-TNB from a 0.5 mg mL^{-1} solution in EtOH. (B) Size distribution for AuNPs-TNB obtained from TEM images.

The characterization of the functionalized AuNPs-TNB was also performed by XPS and confirmed the presence of characteristic functional groups on the surface of the nanoparticles (**Figure S2**). All specific features are shown in **Figure S3**. Spectrum for C(1s) showed peaks at 287.9 eV assigned to –COOH groups and a broad band deconvoluted at 284.4, 285.1 and 286.0 eV assigned to C=C, C-C and C-O/C-N bonds. Oxygen related spectrum (O(1s)) showed contribution for $–NO_2$, O=C, C-OH at 530.7, 532.0 and 532.9 eV respectively while the weak broad band at 534.9 eV was ascribed to partial hydration of the particles (H_2O). Finally, a well-defined peak centered at 405.6 eV for the N(1s) was correlated to $–NO_2$. The composition of the gold nanoparticles was evaluated based on atomic % extracted from deconvoluted spectra and was in good agreement with expected values (S:N:O:C ratio: 0.9:1:4.1:7.5 (found) vs. 1:1:4:7 (expected) relative to N atom).

3.2. Electrochemical characterization of AuNPs-TNB

The electrochemical characterization of the AuNPs-TNB adsorbed on MWCNTs layer was performed in McIl buffer (pH 7.0) with cyclic voltammetry as shown in **Figure 2**. As expected, the AuNPs-TNB were activated electrochemically by reducing the nitro groups located on the outer sphere of the AuNPs as seen from the reduction tail on the CV scans in the cathodic region and starting at -0.300 V. This led to the formation of hydroxylamine groups (-NHOH) shown in equation (1). This reduction was associated with the apparition of the new

system describing the reversible interconversion of the hydroxylamine to the corresponding nitroso group (-NO) centered at $E_{1/2}$ = -0.031 ± 0.005 V according to the global equation (2).

$$\boldsymbol{R-NO_2+4e^-+4H^+ \rightarrow R-NHOH+H_2O} \quad (1)$$

$$\boldsymbol{R-NHOH \leftrightarrow R-NO+2e^-+2H^+} \quad (2)$$

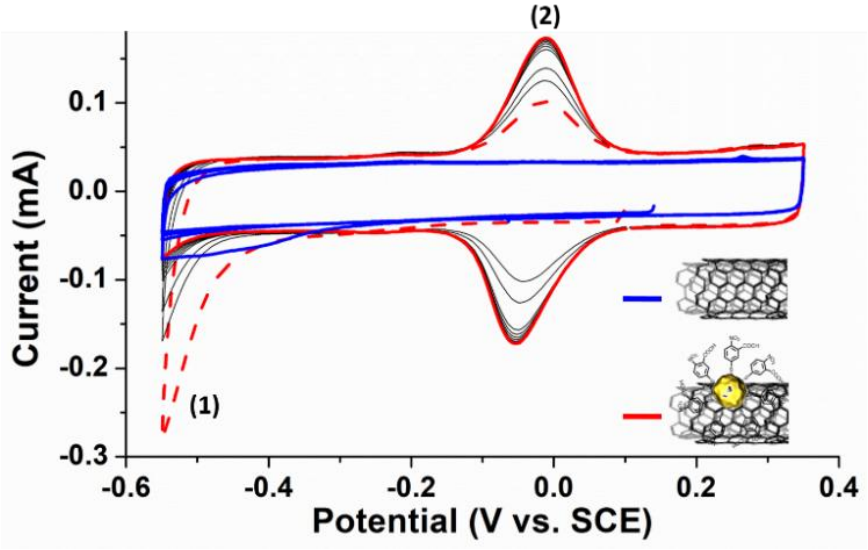

Figure 2: Electrochemical activation of the AuNPs-TNB/MWCNTs electrodes through reduction of the nitro groups by cyclic voltammetry in McIl buffer (pH 7.0) purged with Ar and recorded at 50 mV s^{-1} during (**red dash**) 1st activation scan, (**thin black**) 2nd 4th 6th 8th 10th and (**red solid**) 12th activation scans. (**blue**) CV scan for unmodified MWCNTs electrodes.

Unmodified MWCNTs electrodes polarized accordingly did not show any redox signal in the same electrochemical window. To guarantee a maximal electroactivation of hydroxylamines and stable electroactive layers the potential was continuously swept until the signal at the foot of the wave for the nitro reduction disappeared [15]; this required 10 cycles from 0.35 to -0.55 V vs. SCE. A voltammetry survey at different pH values (from 3.0 to 8.0) exhibited a shift of the calculated $E_{1/2}$ by -65 ± 1.4 mV/pH unit (**Figure S4**). It confirmed the 1:1 ratio for proton/electron exchange and thus the assumption of n = 2 was validated.

Subsequently, cyclic voltammograms performed at different scan rates were used to determine the surface coverage of the activated hydroxylamine (Γ_{NHOH}) at the surface of the electrodes. As the oxidation and the reduction peak currents were linearly dependent on the scan rate (**Figure S5**), the Laviron's equation was used for this purpose (equation (3)).

$$\boldsymbol{I_{pf}=\frac{n^2F^2S\Gamma_{NHOH}}{4RT}v} \quad (3)$$

where I_{pf} is the faradaic peak current, n is the number of electrons involved in the process, F is Faraday's constant, S is the geometric surface area of the CNTs layer, R is the gas constant, T is the temperature, and v is the scan rate. The resulting average Γ_{NHOH} = 8.80 ± 0.60 10^{-9} mol cm^{-2} corresponds to an increase by a factor 50 of the apparent surface coverage obtained by

adsorption of DTNB precursor on MWCNTs (Γ_{DTNB} = 0.16 ± 0.03 10^{-9} mol cm^{-2}). Furthermore, the electroactivity of the activated AuNPs remained stable for a longer period since it retained 50% and 30% of its original activity after 7 and 21 days respectively. As a comparison, this is a drastic improvement compared to the poor stability of the activated DTNB adsorbed on MWCNTs layers where no electrochemical signal was detected after only 4 days (**Figure S6**). The apparent electron transfer (ET) rate, k_{ET} of the AuNPs adsorbed on the MWCNTs layer was calculated by recording cyclic voltammograms up to 15 V s^{-1} and plotting the change in the anodic and cathodic peak potentials as function of log(v) according to the Laviron's model [27] as shown in **Figure 3**.

$$\boldsymbol{k_{ET} = \frac{(1-\alpha)nFv_a}{RT} = \frac{\alpha nFv_c}{RT}} \quad (4)$$

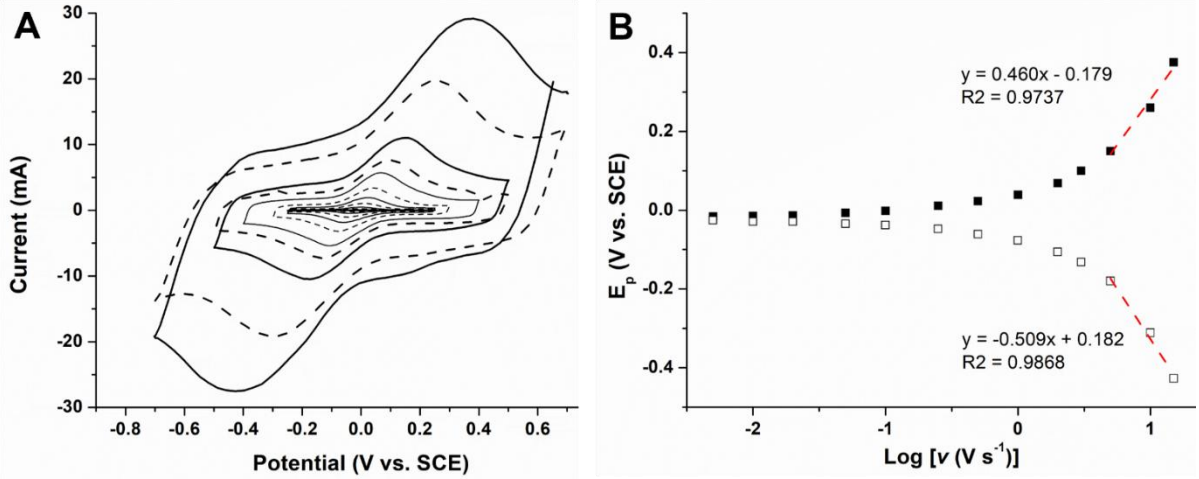

Figure 3: (A) Cyclic voltammograms of activated AuNPs-TNB/MWCNTs electrodes recorded at different scan rates from 0.01 V s^{-1} to 15 V s^{-1} in McIl buffer (pH 7.0). (B) Voltammetric peak potentials *vs.* scan rate for activated AuNPs-TNB/MWCNTs electrodes (■) $E_{p,a}$ and (□) $E_{p,c}$. In red, the linearized portions for k_{ET} determination.

At relatively high scan rates, both anodic and cathodic branches tend to be linear with the variation of log(v) forming two asymptotes with slopes equal to $2.3RT/(1-\alpha)nF$ and $2.3RT/\alpha nF$ respectively. As shown in equation (4), k_{ET} can be obtained when $v_a = v_c$, or more explicitly at the intercept of the two asymptotes mentioned earlier. The apparent ET rate constant for AuNPs-TNB at MWCNTs electrodes was k_{ET} = 12 ± 1 s^{-1}. This value is in the range of several literature reports based on nitroaromatics immobilized on carbon surfaces (from 1.7 s^{-1} to 14 s^{-1}) [17,20,28]. However, it appeared to be slower than another study reported by Kubota et al. utilizing a similar approach (MWCNTs, AuNPs and DTNB) [29]. In their work, k_{ET} achieved 43 s^{-1}. The slower rate could be attributed to the lower purity of the MWCNTs used herein (purity >90%).

3.3.Bioelectroreduction of O_2 at MCO/AuNPs-TNB/MWCNT modified electrodes

The aforementioned unactivated AuNPs-TNB were assessed for the improvement of direct ET of two different MCOs commonly used for their electrocatalytic activity toward oxygen reduction reaction (ORR) (**Figure 4**). Before electrochemical survey for ORR, few electrodes were sacrificed to verify the presence of the AuNPs-TNB after MCO incubation through their electrochemical activation. In N_2 saturated electrolyte, the surface coverage was comparable with regard to the section *3.2.* (I_{pa} = 100 µA during 10^{th} activation scan). Functionalization of the MWCNTs surface with AuNPs did not affect drastically the open circuit potential (OCP) of the bioelectrodes compared to unmodified carbon film (OCP_{lac} = 0.600 ± 30 mV and OCP_{BOx} = 520 ± 30 mV. The small ΔOCP (~ 80 mV) between the two MCOs was attributed to the pH change of the electrolytes. Characterization of the electrocatalytic properties of the bioelectrodes were performed by cyclic voltammetry. Onset potentials for ORR were in agreement with reported literature and again function with the electrolyte pH (E_{lac} = 0.610 V E_{BOx} = 0.530 V). Non-negligible electrocatalytic turnover was recorded based on 1- the MCO used in the study and 2- the degree of functionalization of the MWCNTs surface (unfunctionalized vs. AuNP-TNB-functionalized). In either case, the electrocatalytic currents recorded were superior for the BOx-based bioelectrodes. It appeared that unfunctionalized MWCNTs were not suitable for the proper orientation of Lc as only j_{max} = 68 ± 12 µAcm^{-2} was obtained at 0.1 V while the current reached j_{max} = 544 ± 85 µAcm^{-2} for the BOx electrode. The functionalization step with AuNPs-TNB led to drastic enhancement of the ORR current densities at both electrodes; j_{max} = 480 ± 50 µA cm^{-2} and j_{max} = 920 ± 72 µA cm^{-2} which represents a 7.5-fold and a 2-fold increase for Lc and BOx respectively. The large increase obtained for laccase is attributed to the increase of aromatic species at the CNTs film (due to the benzene ring). The lower increase in current density obtained at BOx/AuNP-TNB could be explained by a "denser" packing of TNB molecule at the AuNP surface (partially hindering electrostatic interaction of the substrate pocket near the T1 Cu center involved in DET). Stability measurements of such BOx-based architecture were assessed daily as they displayed the best performances. After 8 days, the bioelectrodes maintained 60% of their initial activity which is consistent with other AuNP-modified biocathodes [30].

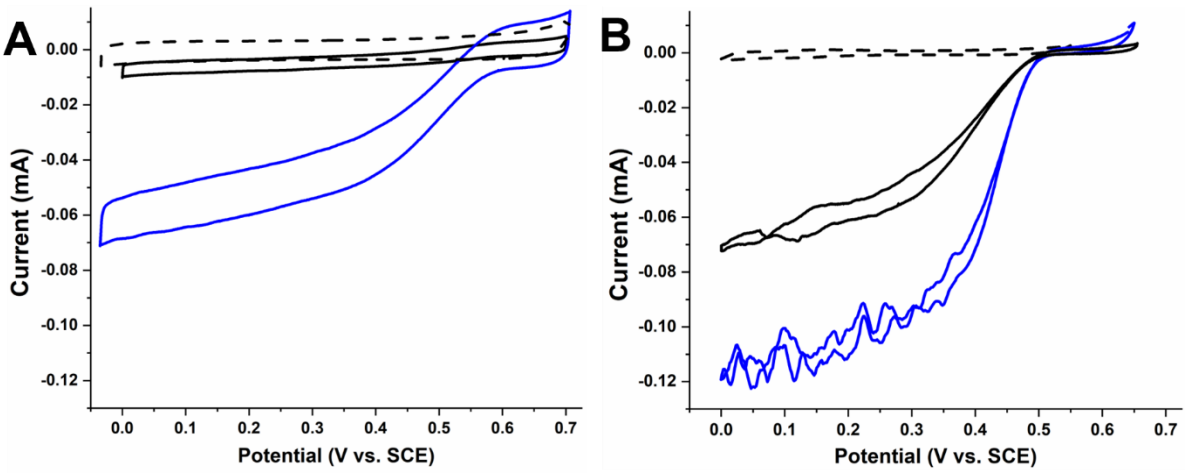

Figure 4: Representative cyclic voltammograms (second scan) for (A) laccase and (B) BOx modified electrodes. MCO/AuNPs-TNB/MWCNT in Ar saturated solution (**dashed line**) and O_2 saturated solution (**blue line**) in McIl buffer [(A) pH 5.0; (B) pH 7.0] at 5 mV s^{-1}. **Solid black lines** represent CV at MCO/MWCNT in O_2 saturated solution. (For interpretation of the references to colors in this figure legend, the reader is referred to the web version of this article).

3.4.Bioelectrooxidation of glucose at GDH/AuNPs-TNB/MWCNT modified electrodes

Activated AuNPs-TNB were also evaluated as electrocatalysts for the oxidation of NADH. In the presence of 2 mmol L^{-1} NADH, the cyclic voltammogram showed an irreversible anodic peak at 0.003 V while the cathodic peak linked to the nitroso reduction disappeared (**Figure S7**). This confirmed the efficient electrocatalytic properties of the synthesized and activated AuNPs-TNB immobilized on MWCNTs surfaces towards the oxidation of NADH. Furthermore, the use of these AuNPs notably enhanced the rate of NADH oxidation compared with its oxidation at unmodified MWCNTs electrodes. This was observed from the shift of the anodic peak potential ($\Delta E_{p,a}$ = -150 mV) of the cofactor reaching diffusion limitation in transient condition and the 1.9-fold increase in $I_{cat,max}$ compared to unmodified MWCNTs electrodes. **Figure S8** presents a control experiment for the electrocatalytic property of unactivated AuNPs-TNB/MWCNTs towards NADH oxidation (BSA was used as a protein model to mimic the adsorption of GDH over the AuNPs layer). It clearly demonstrated that the presence of the protein acts as an insulating layer on the CNTs surface making direct oxidation of NADH on CNTs more difficult. Hence, activated particles are envisioned as key components to afford oxidation of NADH at low potential on NAD-dependent enzyme-modified electrode. Due to the diversity of NAD-dependent dehydrogenases and their known sensitivity to pH conditions, it was necessary to evaluate the ability of the newly synthesized AuNPs to oxidize NADH in different pH solutions. Chronoamperometric measurements were carried out at $E_{pa,\ NHOH}$ in electrolyte ranging from pH 5.0 to pH 8.0 to ensure identical driving force regardless of the $E_{1/2}$ shift due to pH change (**Figure 5**). It shows that best performing conditions are obtained in slightly acidic solutions. Nevertheless, the electrocatalyst can be used in slightly alkaline solutions (pH 8.0) since electrocatalytic current remained 70 % of its maximal performance recorded at pH 5.0.

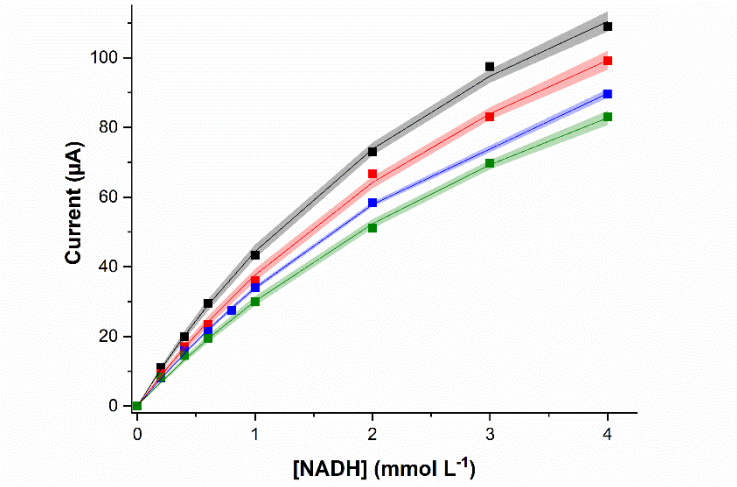

Figure 5: Calibration curves for AuNPs-TNB/MWCNT modified electrodes with increasing concentration of NADH in McIl buffer at various pH: 5.0 (**black**), 6.0 (**red**), 7.0 (**blue**) and 8.0 (**green**) obtained from chronoamperometric measurement performed at $E_{pa,\ NHOH}$.

Consequently, a NAD-dependent glucose dehydrogenase was adsorbed on the AuNPs-TNB/MWCNTs to form a GDH/AuNPs-TNB/MWCNT nanocomposite. An electrocatalytic survey was first performed by cyclic voltammetry (**Figure 6**). In 100 mmol L^{-1} glucose solution, the CV showed a more sigmoidal shape (as opposed to the CV obtained for NADH survey) typical for electrocatalytic behavior in substrate saturating condition.

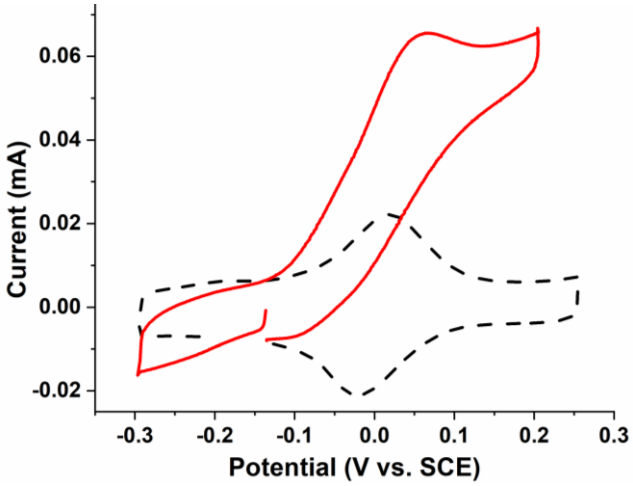

Figure 6: (A) Representative cyclic voltammograms (second scan) of GDH/AuNPs-TNB/MWCNT in 2 mmol L^{-1} NAD^+ (**dashed line**) and in the presence of 100 mmol L^{-1} glucose (**red solid line**) in Ar saturated McIl buffer (pH 7.0) at 5 mV s^{-1}.

Interferent analysis was also carried out to get an assessment of the precision of the proposed architecture. We focused our attention on ascorbic acid (AA), dopamine (DA) and uric acid (UA), three most common interferents found in physiological fluids. It appears that in most cases, minimal glucose level is higher than the maximal concentration reported for each individual interfering compound (**Table S1**). Hence, experiments were performed with

maximal interferent concentration found in body fluids (**Figure S9**). Only AA could lead to a less accurate glucose quantification as its oxidation takes place within the same potential window as the electrocatalysts. On the other hand, DA and UA are oxidized at sufficiently higher potential (> $E_{pa,\ NHOH}$) avoiding parasitic oxidation at our AuNPs-TNB based bioelectrodes.

3.5.AuNPs-TNB/MWCNT modified electrodes for self-powered glucose sensing

Based on previous results, in O_2 saturated solution, the BOx-based biocathode can be combined with the GDH-based bioanode to afford complete glucose/O_2-EFC with no limitation from the cathode before saturation with glucose ($j_{max,\ BOx}$ = 920 ± 72 µA cm^{-2} and $j_{max,\ GDH}$ = 430 ± 24 µA cm^{-2}). This EFC can be utilized to detect and sense glucose in solution based on the power generated by the device. From linear polarization curves of half-cell measurements, a power curve was constructed (**Figure S10**). It shows that the EFC possesses large open circuit voltage (OCV = 0.84 ± 0.02 V) and can sustain power generation in the presence of glucose. In these conditions, it can deliver maximal power density of *ca.* 160 µW cm^{-2} at 0.43 V. The operating potential of the EFC was chosen to ensure maximal polarization of the anode below the oxidation thresholds of DA and UA (hence, not exceeding 0.09 V vs. SCE). The power delivered by the device in the absence of glucose was solely due to the presence of the reduced NHOH on the bioanode surface during the first potential sweep and was not recovered afterwards for subsequent polarizations.

Hence, glucose sensing was performed potentiostatically at this specific voltage. This also ensured mitigation of capacitive current contribution as opposed to the power measurement from polarization curves. To ensure no diffusion limitation during acquisition process and minimal polarization from the biocathode, the solution was moderately stirred. Data were processed with the "adjacent-averaging" method from OriginPro Software to minimize noise contribution (**Figure S11A**). Glucose detection was positive as low as 2.0 µmol L^{-1}. The lower detection limit (LOD) calculated taking in account a 3-fold signal/noise ratio was found to be 2.5 ± 0.9 µmol L^{-1}. The **Figure S11B** depicts the calibration curves obtained upon glucose addition to the electrolyte. The power density response followed a Michaelis-Menten kinetics (K_m = 6.1 ± 0.5 mmol L^{-1}) with a limiting power density (P_{max}) upon enzyme saturation with substrate at P_{max} = 156 ± 15 µW cm^{-2}. In low glucose level (*i.e.* 40 µmol L^{-1} to 4 mmol L^{-1}), the calibration curves displayed a linear regions with average sensitivities of 1.76 (± 0.04) × 10^4 µW L mmol^{-1} cm^{-2} (R^2 = 0.992) (**Figure 7**). This range is of great interest for elucidating glucose concentration in physiological fluids (**Table S1**). From this linearization, the 95% confidence level projection for glucose quantification at a given catalytic current was associated with small errors ranging from ± 0.35 mmol L^{-1} to ± 16 µmol L^{-1} for 4 mmol L^{-1} and 50 µmol L^{-1} respectively. It is below the requirement set by the ISO 15197:2013 standard with accuracy of test strips within ± 0.83 mmol L^{-1} for glucose concentrations lower than 5.6 mmol L^{-1} [31].

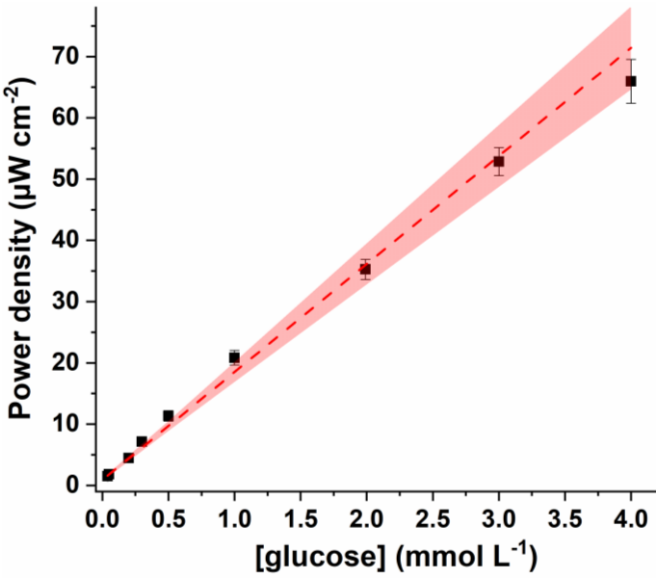

Figure 7: Linear region for glucose sensing reported for AuNPs-TNB based EFCs polarized at 0.43 V. The colored zone depicts the 95% confidence level projection for glucose concentration at any power density (x-axis error).

4. Conclusions

We showed the synthesis of gold nanoparticles containing nitro groups (AuNPs-TNB) and their direct application in bioelectrocatalysis for orientation enhancement of MCOs and for the regeneration of the NAD^+ cofactor required for NAD-glucose dehydrogenase. Herein, we demonstrated their physical, chemical and electrochemical properties from a large variety of characterization techniques. The two different bioelectrodes were combined to afford a glucose/O_2 enzymatic biofuel cell with capabilities for self-powered glucose sensing. The AuNPs-TNB based EFC displayed interesting capabilities in term of current and power generation in high glucose concentration (>50 mmol L^{-1}) reaching *ca.* 420 µA cm^{-2} and 156 µW cm^{-2}. In physiological glucose level, the device was also adapted for accurate glucose sensing with LOD as low as 2.5 µmol L^{-1} and a linear range from 40 µmol L^{-1} to 4 mmol L^{-1}. Further studies will be devoted to rationalize the disulfide structure during AuNP synthesis to adapt the aromatic/electrostatic environments of the particles and to enhance the electrocatalytic activity of the AuNPs.

CRediT authorship contribution statement

Noémie Lalaoui: Conceptualization, Formal analysis, Investigation, Methodology, Visualization, Validation, Writing - review, Supervision. **Kilian Gentil**: Investigation. **Ilyass Ghandari**: Investigation. **Serge Cosnier**: Funding acquisition, Writing - review. **Fabien**

Giroud: Conceptualization, Formal analysis, Investigation, Methodology, Visualization, Validation, Writing – original draft & editing, Supervision.

Declaration of competing interest

There are no conflicts to declare.

Acknowledgements

FG and SC wish to acknowledge the ANR for partial funding of the project. FG and SC greatly thank the support from the platform Chimie NanoBio ICMG FR 2607 (PCN-ICMG) and granting access to the electron microscopy facility. FG and SC also thank the LabEx ARCANE (ANR-11-LABX-0003-01 and CBH-EUR-GS, ANR-17-EURE-0003).

Appendix A. Supplementary information

Supplementary information link to this article can be found online at xxx.

References

[1] H. Chen, F. Dong, S.D. Minteer, The progress and outlook of bioelectrocatalysis for the production of chemicals, fuels and materials, Nat. Catal. 3 (2020) 225–244. https://doi.org/10.1038/s41929-019-0408-2.

[2] S.H. Jee, H. Ohrr, J.W. Sull, J.E. Yun, M. Ji, J.M. Samet, Fasting Serum Glucose Level and Cancer Risk in Korean Men and Women, JAMA. 293 (2005) 194–202. https://doi.org/10.1001/jama.293.2.194.

[3] M. Apicella, M.C. Campopiano, M. Mantuano, L. Mazoni, A. Coppelli, S.D. Prato, COVID-19 in people with diabetes: understanding the reasons for worse outcomes, Lancet Diabetes Endocrinol. 8 (2020) 782–792. https://doi.org/10.1016/S2213-8587(20)30238-2.

[4] C. Jurysta, N. Bulur, B. Oguzhan, I. Satman, T.M. Yilmaz, W.J. Malaisse, A. Sener, Salivary Glucose Concentration and Excretion in Normal and Diabetic Subjects, J. Biomed. Biotechnol. 2009 (2009). https://doi.org/10.1155/2009/430426.

[5] H. Yao, A.J. Shum, M. Cowan, I. Lähdesmäki, B.A. Parviz, A contact lens with embedded sensor for monitoring tear glucose level, Biosens. Bioelectron. 26 (2011) 3290–3296. https://doi.org/10.1016/j.bios.2010.12.042.

[6] X. Xuan, H.S. Yoon, J.Y. Park, A wearable electrochemical glucose sensor based on simple and low-cost fabrication supported micro-patterned reduced graphene oxide nanocomposite electrode on flexible substrate, Biosens. Bioelectron. 109 (2018) 75–82. https://doi.org/10.1016/j.bios.2018.02.054.

[7] B. Scherstén, H. Fritz, Subnormal Levels of Glucose in Urine: A Sign of Urinary Tract Infection, JAMA. 201 (1967) 949–952. https://doi.org/10.1001/jama.1967.03130120057014.

[8] A.A. Karyakin, S.V. Nikulina, D.V. Vokhmyanina, E.E. Karyakina, E.K.H. Anaev, A.G. Chuchalin, Non-invasive monitoring of diabetes through analysis of the exhaled breath condensate (aerosol), Electrochem. Commun. 83 (2017) 81–84. https://doi.org/10.1016/j.elecom.2017.09.005.

[9] R.A. Rincón, C. Lau, H.R. Luckarift, K.E. Garcia, E. Adkins, G.R. Johnson, P. Atanassov, Enzymatic fuel cells: Integrating flow-through anode and air-breathing cathode into a membrane-less biofuel cell design, Biosens. Bioelectron. 27 (2011) 132–136. https://doi.org/10.1016/j.bios.2011.06.029.

[10] R.C. Reid, S.D. Minteer, B.K. Gale, Contact lens biofuel cell tested in a synthetic tear solution, Biosens. Bioelectron. 68 (2015) 142–148. https://doi.org/10.1016/j.bios.2014.12.034.

[11] A. de S. Santos, L. Gorton, L.T. Kubota, Electrocatalytic NADH Oxidation Using an Electrode Based on Meldola Blue Immobilized on Silica Coated with Niobium Oxide, Electroanalysis. 14 (2002) 805–812. https://doi.org/10.1002/1521-4109(200206)14:12<805::AID-ELAN805>3.0.CO;2-P.
[12] A.A. Karyakin, E.E. Karyakina, W. Schuhmann, H.-L. Schmidt, S.D. Varfolomeyev, New amperometric dehydrogenase electrodes based on electrocatalytic NADH-oxidation at poly (methylene blue)-modified electrodes, Electroanalysis. 6 (1994) 821–829. https://doi.org/10.1002/elan.1140061003.
[13] C.-X. Cai, K.-H. Xue, Electrocatalysis of NADH oxidation with electropolymerized films of azure I, J. Electroanal. Chem. 427 (1997) 147–153. https://doi.org/10.1016/S0022-0728(96)04996-0.
[14] B. Reuillard, A. Le Goff, S. Cosnier, Non-covalent double functionalization of carbon nanotubes with a NADH oxidation Ru(II)-based molecular catalyst and a NAD-dependent glucose dehydrogenase, Chem. Commun. 50 (2014) 11731–11734. https://doi.org/10.1039/C4CC04758C.
[15] E. Casero, M. Darder, K. Takada, H.D. Abruña, F. Pariente, E. Lorenzo, Electrochemically Triggered Reaction of a Surface-Confined Reagent: Mechanistic and EQCM Characterization of Redox-Active Self-Assembling Monolayers Derived from 5,5‘-Dithiobis(2-nitrobenzoic acid) and Related Materials, Langmuir. 15 (1999) 127–134. https://doi.org/10.1021/la9806552.
[16] N. Mano, A. Kuhn, Immobilized nitro-fluorenone derivatives as electrocatalysts for NADH oxidation, J. Electroanal. Chem. 477 (1999) 79–88. https://doi.org/10.1016/S0022-0728(99)00393-9.
[17] R. Moscoso, E. Inostroza, S. Bollo, J.A. Squella, Electrocatalysis of NADH on 3,5-Dinitrobenzoic Acid Encapsulated on Multiwalled Carbon Nanotube-Modified Electrode, Electrocatalysis. 7 (2016) 357–361. https://doi.org/10.1007/s12678-016-0323-0.
[18] M. Santhiago, P.R. Lima, W. de J.R. Santos, A.B. de Oliveira, L.T. Kubota, In situ activated 3,5-dinitrobenzoic acid covalent attached to nanostructured platform for NADH electrooxidation, Electrochimica Acta. 54 (2009) 6609–6616. https://doi.org/10.1016/j.electacta.2009.06.032.
[19] F. Giroud, K. Sawada, M. Taya, S. Cosnier, 5,5-Dithiobis(2-nitrobenzoic acid) pyrene derivative-carbon nanotube electrodes for NADH electrooxidation and oriented immobilization of multicopper oxidases for the development of glucose/O2 biofuel cells, Biosens. Bioelectron. 87 (2017) 957–963. https://doi.org/10.1016/j.bios.2016.09.054.
[20] R. Moscoso, C. Barrientos, S. Moris, J.A. Squella, Electrocatalytic oxidation of NADH in a new nanostructured interface with an entrapped butylpyrene nitroaromatic derivative, J. Electroanal. Chem. 837 (2019) 48–54. https://doi.org/10.1016/j.jelechem.2019.02.013.
[21] E.-S. Jeong, M. Sathishkumar, R. Jayabalan, S.-H. Jeong, S.-Y. Park, S.-P. Mun, S.-E. Yun, Immobilization of a mediator onto carbon cloth electrode and employment of the modified electrode to an electroenzymatic bioreactor, J. Microbiol. Biotechnol. 22 (2012) 1406–1411.
[22] C. Gutiérrez-Sánchez, M. Pita, C. Vaz-Domínguez, S. Shleev, A.L. De Lacey, Gold Nanoparticles as Electronic Bridges for Laccase-Based Biocathodes, J. Am. Chem. Soc. 134 (2012) 17212–17220. https://doi.org/10.1021/ja307308j.
[23] O. Swiech, N. Hrynkiewicz-Sudnik, B. Palys, A. Kaim, R. Bilewicz, Gold Nanoparticles Tethered to Gold Surfaces Using Nitroxyl Radicals, J. Phys. Chem. C. 115 (2011) 7347–7354. https://doi.org/10.1021/jp200842u.
[24] I. Hussain, S. Graham, Z. Wang, B. Tan, D.C. Sherrington, S.P. Rannard, A.I. Cooper, M. Brust, Size-Controlled Synthesis of Near-Monodisperse Gold Nanoparticles in the 1−4 nm Range Using Polymeric Stabilizers, J. Am. Chem. Soc. 127 (2005) 16398–16399. https://doi.org/10.1021/ja055321v.
[25] S. Chen, K. Kimura, Synthesis and Characterization of Carboxylate-Modified Gold Nanoparticle Powders Dispersible in Water, Langmuir. 15 (1999) 1075–1082. https://doi.org/10.1021/la9812828.
[26] C.E. Anson, C.S. Creaser, G. Richard Stephenson, FTIR study of π-stacking effects in (η6-arene)tricarbonylchromium complexes: application as a molecular sensor for aromatic analytes, Spectrochim. Acta. A. Mol. Biomol. Spectrosc. 52 (1996) 1183–1191. https://doi.org/10.1016/0584-8539(96)01678-9.

[27] E. Laviron, L. Roullier, General expression of the linear potential sweep voltammogram for a surface redox reaction with interactions between the adsorbed molecules: Applications to modified electrodes, J. Electroanal. Chem. Interfacial Electrochem. 115 (1980) 65–74. https://doi.org/10.1016/S0022-0728(80)80496-7.
[28] C.C. Corrêa, M. Santhiago, A.L.B. Formiga, L.T. Kubota, In situ activated nanostructured platform for oxidized glutathione biosensing, Electrochimica Acta. 90 (2013) 309–316. https://doi.org/10.1016/j.electacta.2012.12.046.
[29] M. Santhiago, P.R. Lima, W. de J.R. Santos, L.T. Kubota, An amperometric sensor for l-cysteine based on nanostructured platform modified with 5,5′-dithiobis-2-nitrobenzoic acid (DTNB), Sens. Actuators B Chem. 146 (2010) 213–220. https://doi.org/10.1016/j.snb.2010.02.051.
[30] N. Lalaoui, P. Rousselot-Pailley, V. Robert, Y. Mekmouche, R. Villalonga, M. Holzinger, S. Cosnier, T. Tron, A. Le Goff, Direct Electron Transfer between a Site-Specific Pyrene-Modified Laccase and Carbon Nanotube/Gold Nanoparticle Supramolecular Assemblies for Bioelectrocatalytic Dioxygen Reduction, ACS Catal. 6 (2016) 1894–1900. https://doi.org/10.1021/acscatal.5b02442.
[31] N. Jendrike, A. Baumstark, U. Kamecke, C. Haug, G. Freckmann, ISO 15197: 2013 Evaluation of a Blood Glucose Monitoring System's Measurement Accuracy:, J. Diabetes Sci. Technol. (2017). https://doi.org/10.1177/1932296817727550.